Kangas, T, Fruchter, AS, Cenko, SB, Corsi, A, de Ugarte Postigo, A, Pe'er, A, Vogel, SN, Cucchiara, A, Gompertz, B, Graham, J, Levan, A, Misra, K, Perley, DA, Racusin, J and Tanvir, N

The Late-time Afterglow Evolution of Long Gamma-Ray Bursts GRB 160625B and GRB 160509A

Draft version April 8, 2020
Typeset using LaTeX **twocolumn** style in AASTeX62

The late-time afterglow evolution of long gamma-ray bursts GRB 160625B and GRB 160509A

Tuomas Kangas,[1] Andrew S. Fruchter,[1] S. Bradley Cenko,[2,3] Alessandra Corsi,[4]
Antonio de Ugarte Postigo,[5,6] Asaf Pe'er,[7] Stuart N. Vogel,[8] Antonino Cucchiara,[9] Benjamin Gompertz,[10]
John Graham,[11] Andrew Levan,[10] Kuntal Misra,[12] Daniel A. Perley,[13] Judith Racusin,[2] and Nial Tanvir[14]

[1]*Space Telescope Science Institute, 3700 San Martin Drive, Baltimore, MD 21218, USA*
[2]*Astrophysics Science Division, NASA Goddard Space Flight Center, Mail Code 661, Greenbelt, MD 20771, USA*
[3]*Joint Space-Science Institute, University of Maryland, College Park, MD 20742, USA*
[4]*Department of Physics and Astronomy, Texas Tech University, Box 1051, Lubbock, TX 79409-1051, USA*
[5]*Instituto de Astrofísica de Andalucía, Glorieta de la Astronomía s/n, E-18008, Granada*
[6]*Dark Cosmology Centre, Niels Bohr Institute, Juliane Maries Vej 30, Copenhagen Ø, 2100, Denmark*
[7]*Department of Physics, Bar-Ilan University, Ramat-Gan 52900, Israel*
[8]*Department of Astronomy, University of Maryland, College Park, MD 20742, USA*
[9]*University of Virgin Islands, College of Science and Mathematics, #2 Brewers Bay Road, Charlotte Amalie, USV1 00802*
[10]*Department of Physics, University of Warwick, Coventry, CV4 7AL, UK*
[11]*Kavli Institute for Astronomy and Astrophysics, Peking University, Beijing 100871, PR China*
[12]*Aryabhatta Research Institute of Observational Sciences (ARIES), Manora Peak, Nainital 263 002, India*
[13]*Astrophysics Research Institute, Liverpool John Moores University, IC2, Liverpool Science Park, 146 Brownlow Hill, Liverpool L3 5RF, UK*
[14]*University of Leicester, Department of Physics & Astronomy and Leicester Institute of Space & Earth Observation University Road, Leicester, LE1 7RH UK*

(Received 2019; Revised 2020; Accepted 2020)

ABSTRACT

We present post-jet-break *HST*, VLA and *Chandra* observations of the afterglow of the long γ-ray bursts GRB 160625B (between 69 and 209 days) and GRB 160509A (between 35 and 80 days). We calculate the post-jet-break decline rates of the light curves, and find the afterglow of GRB 160625B inconsistent with a simple $t^{-3/4}$ steepening over the break, expected from the geometric effect of the jet edge entering our line of sight. However, the favored optical post-break decline ($f_\nu \propto t^{-1.96\pm0.07}$) is also inconsistent with the $f_\nu \propto t^{-p}$ decline (where $p \approx 2.3$ from the pre-break light curve), which is expected from exponential lateral expansion of the jet; perhaps suggesting lateral expansion that only affects a fraction of the jet. The post-break decline of GRB 160509A is consistent with both the $t^{-3/4}$ steepening and with $f_\nu \propto t^{-p}$. We also use BOXFIT to fit afterglow models to both light curves and find both to be energetically consistent with a millisecond magnetar central engine, although the magnetar parameters need to be extreme (i.e. $E \sim 3 \times 10^{52}$ erg). Finally, the late-time radio light curves of both afterglows are not reproduced well by BOXFIT and are inconsistent with predictions from the standard jet model; instead both are well represented by a single power law decline (roughly $f_\nu \propto t^{-1}$) with no breaks. This requires a highly chromatic jet break ($t_{j,\rm radio} > 10 \times t_{j,\rm optical}$) and possibly a two-component jet for both bursts.

Keywords: gamma-ray burst: general — gamma-ray burst: individual (GRB 160625B; GRB 160509A) — relativistic processes

1. INTRODUCTION

Gamma-ray bursts (GRBs) are among the most luminous transient events in the universe. Through their association with broad-lined type Ic supernovae (e.g. Iwamoto et al. 1998; Woosley & Bloom 2006; Hjorth & Bloom 2012), long GRBs (LGRBs; duration of the

Corresponding author: Tuomas Kangas
tkangas@stsci.edu

prompt γ-ray emission more than 2 s) have been established as the terminal core-collapse explosions of massive stars at cosmological distances (e.g. Paczynski 1986; Woosley 1993; MacFadyen & Woosley 1999), where an ultra-relativistic jet is launched and breaks out of the stellar envelope, generating the initial prompt emission of γ rays through an as yet unclear mechanism (for a review on GRB physics, see e.g. Piran 2004; Kumar & Zhang 2015). The central engine responsible for launching the jet and powering the emission may be either accretion onto a black hole formed in the core collapse (Woosley 1993) or rotational energy released through the spin-down of a nascent magnetar (e.g. Bucciantini et al. 2008, 2009). The prompt emission of a GRB is followed by an afterglow from X-ray to radio frequencies – synchrotron emission from an external shock created by the interaction between the circumburst medium (CBM) and the highly collimated and relativistically beamed jet (e.g. Paczynski & Rhoads 1993; Sari et al. 1998; Piran 2004). The flux density of the afterglow declines as a power law of the form $f_\nu \propto t^\alpha$.

As the jet interacts with the CBM, it decelerates and the relativistic beaming effect diminishes over time (on the order of days or weeks after a long GRB; e.g. Racusin et al. 2009). This results in an achromatic *jet break* in the afterglow light curve when the relativistic beaming angle (Γ^{-1}, where Γ is the bulk Lorentz factor in the jet) becomes comparable to the opening angle of the jet (Rhoads 1999; Sari et al. 1999), with a steeper power-law decline after the break. The post-break decline is affected by a geometric 'edge effect', in contrast to the situation pre-break where the observer only sees a fraction of the jet front and hence behaviour consistent with an isotropic fireball model. This phenomenon is believed to steepen the decline slope α by $-3/4$ over the break assuming a constant-density CBM, or by $-1/2$ in the case of a wind-like CBM (e.g. Mészáros & Rees 1999; Panaitescu & Mészáros 1999; Kumar & Zhang 2015). Another effect is that, around the same time as this happens, transverse sound waves become able to cross the jet and lateral expansion starts, exponentially decelerating the shock wave. Theoretically the post-break slope in this scenario is expected to be equal to $-p$ (e.g. Sari et al. 1999), where p is the index of the electron Lorentz factor distribution ($N(\gamma) \propto \gamma^{-p}$), typically estimated to be between 2 and 3. There is, however, evidence from numerical simulations that the lateral expansion is unimportant until a later stage – at least unless the jet is very narrow, $\theta_j \lesssim 3$ deg (Lyutikov 2012; Granot & Piran 2012). At even later times, the jet is expected to be better described as a non-relativistic fireball in the Sedov-von Neumann-Taylor regime, resulting in a somewhat flatter decline (e.g. Frail et al. 2000; van der Horst et al. 2008).

Simulations of relativistic shocks have resulted in values around $p \approx 2.2$ (e.g. Bednarz & Ostrowski 1998; Gallant et al. 1999; Kirk et al. 2000). In the X-rays, the pre-break light curve tends to follow a decline around $t^{-1.2}$ (albeit with some variation; e.g. Piran 2004; Zhang et al. 2006); thus both of these effects result in a roughly similar post-break decline (i.e. $\sim t^{-2}$, though with high uncertainties due to the the fast decline and the resulting faintness; often there are not enough data to distinguish between $t^{-1.9}$ and $t^{-2.2}$). Thus determining the exact scenario observationally requires late-time observations of the rapidly declining afterglows to constrain this slope.

The Large Area Telescope (LAT) on the *Fermi* Gamma-ray Space Telescope has detected a number of GRBs at relatively high energies (MeV to GeV) since the launch of *Fermi* in 2008. These are often among the most energetic GRBs, consistent with the Amati correlation between isotropic-equivalent energy $E_{\rm iso}$ and the peak of the energy spectrum (Amati et al. 2002), and can haveisotropic-equivalent energies on the order of 10^{54} erg (Cenko et al. 2011). Some of these most energetic bursts do not exhibit the expected jet breaks, suggesting larger opening angles than expected and making them even more energetic intrinsically (De Pasquale et al. 2016; Gompertz & Fruchter 2017). With beaming-corrected energies on the order of 10^{52} erg, magnetar spin-down models struggle to produce the required power (Cenko et al. 2011). Thus examining the late-time evolution of the LAT bursts can shed light on the physics of the most energetic GRBs.

In this paper, we present results from our late-time *Hubble Space Telescope* (*HST*), Karl G. Jansky Very Large Array (VLA) and *Chandra X-ray Observatory* imaging observations of the afterglows of two LAT bursts, GRB 160625B and GRB 160509A. GRB 160625B was discovered by the Gamma-ray Burst Monitor (GBM) on *Fermi* on 2016 June 25 at 22:40:16.28 UT (MJD 57564.9; Dirirsa et al. 2016) and detected by the LAT as well. Xu et al. (2016) determined its redshift to be $z = 1.406$. It was one of the most energetic γ-ray bursts ever observed with $E_{iso} \sim 3 \times 10^{54}$ erg (Wang et al. 2017; Zhang et al. 2018), and a well-studied object with a multi-frequency follow-up that revealed signs of a reverse shock within the jet (Alexander et al. 2017). The jet break time was unusually long, around 20 days, as expected from unusually bright GRBs (the median time is ~ 1 d, with more energetic bursts having longer break times; see Racusin et al. 2009). GRB 160509A was detected by GBM and LAT on 2016 May

9 at 08:59:04.36 UT (MJD 57517.4; Roberts et al. 2016; Longo et al. 2016a,b) at a redshift of $z = 1.17$ (Tanvir et al. 2016). With $E_{iso} = 8.6 \pm 1.1 \times 10^{53}$ erg, this was another luminous burst that exhibited signs of a reverse shock as well (Laskar et al. 2016).

Our observations of GRB 160625B make its follow-up one of the longest post-jet-break optical and X-ray follow-ups of a GRB afterglow[1], thus providing one of the best estimates of the post-break decline in these bands so far, while for GRB 160509A no prior estimates of the infrared/optical post-break decline could be made due to the very sparse light curve.

Our observations and data reduction process are described in Section 2. Our analysis and results are presented in Section 3. In Section 4, we discuss the implications of our findings, and finally present our conclusions in Section 5. All magnitudes are in the AB magnitude system (Oke & Gunn 1983) and all error bars correspond to 1σ confidence intervals. We use the cosmological parameters $H_0 = 69.6$ km s^{-1} Mpc^{-1}, $\Omega_m = 0.286$ and $\Omega_\Lambda = 0.714$ (Bennett et al. 2014).

2. OBSERVATIONS AND DATA REDUCTION

Late-time imaging observations of GRB 160625B were performed using *HST*/WFC3 and the F606W filter on 2016 September 5 (71.5 d) and 2016 November 13 (140.2 d). A template image of the host galaxy was created by combining images obtained with the same setup on 2017 November 6 (498.3 d) and 11 (503.6 d). At this time the contribution of the afterglow itself was a factor of ~ 13 fainter than at 140 d, assuming a $f_\nu \propto t^\alpha$ decline where $\alpha = -2$. Imaging of GRB 160509A in the H band was performed using the Canarias InfraRed Camera Experiment (CIRCE; Eikenberry et al. 2018) instrument on Gran Telescopio Canarias (GTC) on 2016 May 15 (5.8 d) and 2016 June 3 (24.8 d). Late-time imaging of GRB 160509A was done using *HST*/WFC3 and the F110W and F160W filters on 2016 June 13 (35.3 d); template images of the host galaxy in these filters were obtained on 2017 July 5 (422.1 d), when, assuming $\alpha = -2$, the afterglow was a factor of 143 fainter. Our *HST* observations of both bursts were executed as part of program GO 14353 (PI Fruchter), and these data are available at 10.17909/t9-yvpg-xb33 (GRB 160625B) and 10.17909/t9-11cx-cv41 (GRB 160509A).

Basic reduction and flux calibration of the *HST* images was performed by the *HST* CALWF3 pipeline. The calibrated images were corrected for distortion, drizzled (Fruchter & Hook 2002) and aligned to a common world coordinate system using the `astrodrizzle`, `tweakreg` and `tweakback` tasks in the DRIZZLEPAC[2] package in PYRAF[3]. The two epochs of GRB 160625B in November 2017 were combined into one template image. Subtraction of the template images and aperture photometry of the afterglows were done using IRAF[4]. Basic reduction of the GTC/CIRCE data was done using standard IRAF tasks. The *HST* F160W template image was subtracted from the CIRCE images using the ISIS 2.2 package (Alard & Lupton 1998; Alard 2000). Flux calibration was done using field stars in the Two-Micron All Sky Survey (2MASS) catalog[5] (Skrutskie et al. 2006), and aperture photometry was performed using standard IRAF tasks. At 24.8 d, we were unable to detect the afterglow and only obtained a (3σ) limit of $H \geq 21.9$ mag.

The measured magnitudes of GRB 160625B were corrected for over-subtraction caused by the continued presence of a faint afterglow in the template image. Assuming a post-jet-break decline of $\alpha = -2.0 \pm 0.2$ (obtained from a single-power-law fit to *uncorrected* > 25 d data, with errors rounded up to be conservative), the afterglow flux present in the template image was estimated to be 2.0 ± 1.0 per cent of the flux at 71.5 d or 7.5 ± 2.6 per cent of the flux at 140.2 d, and thus the images at these epochs were over-subtracted by approximately these amounts. The magnitudes were adjusted for this; the errors of the corrected magnitudes include an estimate of the uncertainty of the over-subtraction. The magnitudes of GRB 160509A were not corrected, as the contribution of the afterglow in the template image was only estimated to be 0.7 per cent of the 35.3 d brightness. The log of optical observations and measured and corrected magnitudes of GRB 160625B are presented in Table 1, while Table 2 contains the near-infrared observations of GRB 160509A. Figure 1 shows our F606W band images and the resulting template subtractions of GRB 160625B, while Figure 2 shows the F160W image and subtraction of GRB 160509A.

Late-time X-ray imaging of both GRBs was performed using *Chandra*/ACIS-S in VFAINT mode (proposal ID 17500753, PI Fruchter). GRB 160625B was observed on 2016 September 3 (69.8 d), 2016 November 15 (142.3 d)

[1] The post-break light curve of GRB 060729 (Grupe et al. 2010) and GRB 170817A (Hajela et al. 2019) has been followed up longer, while GRB 130427A was followed for ~ 1000 days (De Pasquale et al. 2016), but exhibited no jet break.

[2] http://drizzlepac.stsci.edu/

[3] http://www.stsci.edu/institute/software_hardware/pyraf

[4] IRAF is distributed by the National Optical Astronomy Observatory, which is operated by the Association of Universities for Research in Astronomy (AURA) under cooperative agreement with the National Science Foundation.

[5] http://www.ipac.caltech.edu/2mass/

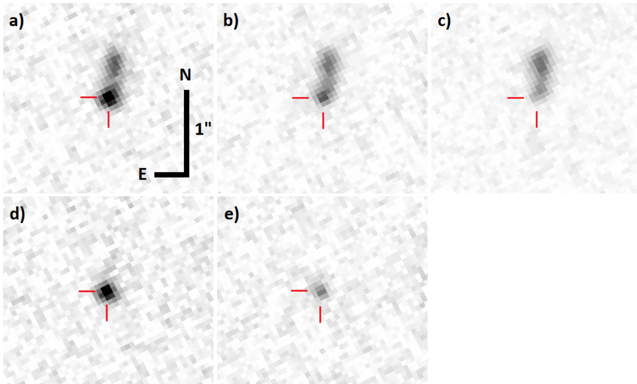

Figure 1. Afterglow and host galaxy of GRB 160625B in the F606W band. *Panel a*: the afterglow and the host galaxy at 71.5 d; *b*: 140.2 d; *c*: the combined template at $\sim$ 500 d; *d*: the template-subtracted image at 71.5 d; and *e*: the subtraction at 140.2 d. North is up and East is to the left in all panels. The black North-South line corresponds to one arcsecond. The afterglow location is indicated with red tick-marks.

and 2016 November 19 (146.2 d). The latter two epochs were combined to obtain the flux at 144.3 ± 2.2 d, as the flux of the afterglow was not expected to vary significantly over a few days at this time. GRB 160509A was observed on 2016 June 20 (42.1 d). Reprocessing of the Chandra level 1 data was performed using the `chandra_repro` script within the CIAO v. 4.9 software (CALDB v. 4.7.7; Fruscione et al. 2006), and aperture photometry was done using IRAF. The web-based Portable Interactive Multi-Mission Simulator (PIMMS[6]) was used to convert count rates in the 0.3 – 10 keV range to unabsorbed flux densities at 5 keV. For GRB 160625B, we used a Galactic neutral hydrogen column density $N_{\rm H,MW} = 9.76 \times 10^{20}$ cm^{-2} (Willingale et al. 2013), a photon index of $\Gamma_X = 1.86$ and an intrinsic absorption of $N_{\rm H,int} = 2.1 \times 10^{21}$ cm^{-2} as derived by Alexander et al. (2017). These parameters are also consistent with the initial analysis by Melandri et al. (2016). For GRB 160509A, we used a Galactic neutral hydrogen column density $N_{\rm H,MW} = 2.12 \times 10^{21}$ cm^{-2} (Willingale et al. 2013), a photon index of $\Gamma_X = 2.07$ and an intrinsic absorption of $N_{\rm H,int} = 1.52 \times 10^{22}$ cm^{-2}, following Laskar et al. (2016). Γ_X is assumed to be constant over the light curve break. The log of X-ray observations and derived flux densities is presented in Table 3.

GRB 160625B was observed in the radio using the VLA in the C, K, X and/or Ku bands at five epochs between 2016 March 30 (4.5 d) and 2017 January 20 (209.0 d), and GRB 160509A in the C and X bands on 2016 June 2 (23.9 d), 2016 June 15 (36.9 d) and 2016 July 28 (79.9 d) (program IDs S81171 and SH0753, PI Cenko and Fruchter respectively). The observations were done in the B configuration, apart from the last GRB 160625B point where configuration A was used. The log of our observations is presented in Table 4. The data were reduced using the Common Astronomy Software Applications package (CASA; McMullin et al. 2007)[7]. Calibration was carried out using the standard VLA calibration pipeline provided in CASA. For GRB 160625B we used J2049+1003 as our complex gain calibrator and 3C48 as our flux and bandpass calibrator. For GRB 160509A we used J2005+7752 as our complex gain calibrator and 3C48 as our flux and bandpass calibrator. After calibration, the data were manually inspected for radio-frequency interference flagging. Imaging was carried out using the `clean` algorithm in interactive mode in CASA. Flux densities reported in Table 4 correspond to peak flux densities measured in a circular region centered on the GRB position, with radius comparable to the nominal full width half maximum of the VLA synthesized beam in the appropriate configuration and frequency band. The reported errors include the VLA cal-

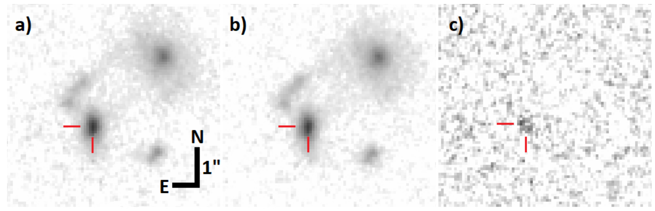

Figure 2. Afterglow and host galaxy of GRB 160509A in the F160W band. *Panel a*: the afterglow and the host galaxy at 35.3 d; *b*: the template at 422.1 d; *c*: the template-subtracted image at 35.3 d. North is up and East is to the left in all panels. The black North-South line corresponds to one arcsecond. The afterglow location is indicated with red tick-marks. The afterglow is very weak compared to the host galaxy, making a template subtraction crucial for this target.

Table 1. Log of our late-time *HST*/WFC3 observations of GRB 160625B.

Phase (d)	MJD	$t_{\rm exp}$ (s)	F606W (mag)	corrected F606W (mag)
71.5	57636.4	2400	25.38 ± 0.03	25.36 ± 0.04
140.2	57705.1	4800	26.76 ± 0.06	26.67 ± 0.07
498.3	58063.2	4800	...	...
503.6	58068.5	4800	...	...

[6] https://heasarc.gsfc.nasa.gov/docs/software/tools/pimms.html

[7] https://casa.nrao.edu

Table 2. Log of our late-time *HST*/WFC3 and GTC/CIRCE observations of GRB 160509A.

Phase (d)	MJD	$t_{\rm exp,F110W}$ (s)	F110W (mag)	$t_{\rm exp,F160W}$ (s)	F160W (mag)	$t_{{\rm exp},H}$ (s)	H (mag)
5.8	57523.2	...	...	...	...	3060	20.50 ± 0.17
24.8	57542.2	...	...	...	...	2100	≥ 21.9
35.3	57552.7	2697	27.11 ± 0.10	2797	26.07 ± 0.07	...	...
422.1	57939.5	2697	...	2797	...	...	...

Table 3. Log of our late-time *Chandra*/ACIS-S observations of GRB 160625B and GRB 160509A.

Phase (d)	MJD	$t_{\rm exp}$ (ks)	f_ν(5 keV) (erg s^{-1} cm^{-2} keV^{-1})
160625B			
69.8	57634.7	19.80	$(1.47 \pm 0.29) \times 10^{-15}$
142.3	57707.3	45.84	...
144.3 ± 2.2[a]	57709.3 ± 2.2	69.56	$(3.21 \pm 0.79) \times 10^{-16}$
146.2	57711.2	23.72	...
160509A			
42.1	57559.5	24.75	$(1.38 \pm 0.25) \times 10^{-15}$

[a]Combination of the 142.3 and 146.2 d epochs.

ibration uncertainty, which is assumed to be 5 per cent below 18 GHz and 10 per cent above it[8].

3. ANALYSIS

3.1. *GRB 160625B*

As our *HST* observations took place after the jet break, we combined our data set with earlier ground-based observations. Both Alexander et al. (2017) and Troja et al. (2017) have published SDSS r' band light curves of GRB 160625B. However, there is a slight ($\sim$ 0.1 mag) systematic offset between these data, so in our light curve fits we have only used the Troja et al. (2017) data set, which has a larger number of data points and which was directly tied to the PanSTARRS magnitude system. Magnitudes of GRB 160625B in the r' band were converted to flux density at the central wavelength of the F606W filter (5947 Å) assuming a spectral slope of $f_\nu \propto \nu^{-0.68}$ between the characteristic synchrotron frequency ν_m and the cooling frequency ν_c (Alexander et al. 2017). As the optical spectrum with $\beta = -0.68 \pm 0.07$ is consistent with the expected index of $\beta = -0.65$ when $p = 2.3$ (also consistent with the light curve; see Section 4.2.1), host extinction is assumed to be negligible. Optical fluxes have been corrected for Galactic reddening, $E(B-V) = 0.1107$ mag (Schlafly & Finkbeiner 2011), assuming the Cardelli et al. (1989)

Table 4. Log of our VLA radio observations of GRB 160625B and GRB 160509A. The GRB 160625B points until 31.3 d were also reported in Troja et al. (2017), but without the calibration uncertainty.

Phase (d)	MJD	ν (GHz)	f_ν (μJy)	Configuration
160625B				
4.5	57569.4	4.8	104 ± 16	B
4.5	57569.4	7.4	454 ± 27	B
4.5	57569.4	19	278 ± 35	B
4.5	57569.4	25	204 ± 36	B
13.4	57578.3	4.8	377 ± 25	B
13.4	57578.3	7.4	310 ± 21	B
13.4	57578.3	22	163 ± 20	B
31.3	57596.2	7.4	113 ± 16	B
31.3	57596.2	22	88 ± 19	B
58.3	57623.2	6.1	75 ± 11	B
58.3	57623.2	22	52 ± 13	B
209.0	57773.9	6.1	16 ± 5	A
160509A				
23.9	57541.3	6.0	80 ± 8	B
23.9	57541.3	9.0	71 ± 7	B
36.9	57554.3	5.0	50 ± 7	B
36.9	57554.3	6.9	52 ± 7	B
36.9	57554.3	8.5	41 ± 6	B
36.9	57554.3	9.5	29 ± 6	B
79.9	57597.3	6.0	27 ± 6	B
79.9	57597.3	9.0	25 ± 5	B

extinction law. In the X-ray, we combined our *Chandra* data with the GRB 160625B light curve from the *Swift*/XRT lightcurve repository[9] (Evans et al. 2007, 2009), converted to 5 keV flux densities using PIMMS as described in Section 2.

We then fitted a smooth broken power law of the form

$$f_\nu = f_{\nu,0}\left[\left(\frac{t}{t_j}\right)^{-\omega\alpha_1} + \left(\frac{t}{t_j}\right)^{-\omega\alpha_2}\right]^{-\frac{1}{\omega}} \quad (1)$$

to the light curve, where t_j is the jet break time, α_1 is the pre-break power-law slope, α_2 the post-break slope,

[8] (https://science.nrao.edu/facilities/vla/docs/manuals/oss/performance/fdscale)

[9] http://www.swift.ac.uk/xrt_curves/

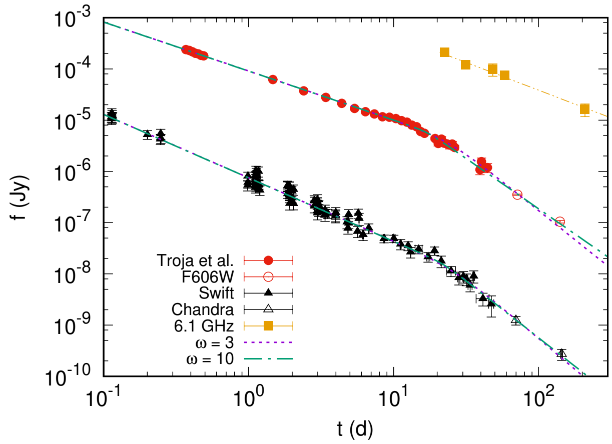

Figure 3. Observed optical (extinction-corrected), X-ray and interpolated 6.1 GHz light curve of the afterglow of GRB 160625B (points) and our power law fits including the broken power laws described by Eq. 1 (lines). The r'-band magnitudes from Troja et al. (2017) (solid circles) have been converted into flux density. X-ray flux densities from *Swift*/XRT (solid triangles) and *Chandra*/ACIS-S (open triangles) are reported at 5 keV. The post-break fit is better assuming $\omega = 10$ (dot-dashed green line), especially regarding the optical *HST* point at 140.2 d. The pre-break fit does not depend on the choice of ω.

and ω describes the sharpness of the break. We fitted this function to both the optical and the X-ray curve using two values, 3 and 10, for ω (a value of 3 was found consistent with most GRB observations by Liang et al. 2007, but some events were found to require a sharper break with $\omega = 10$). The results of the fit parameters are presented in Table 5. The pre-break decline α_1 does not depend on the choice of ω; we found $\alpha_{1,\mathrm{F606W}} = -0.96 \pm 0.01$ and $\alpha_{1,\mathrm{X}} = -1.24 \pm 0.02$ in both cases. The best fit to the post-break decline was $\alpha_{2,\mathrm{F606W}} = -2.27 \pm 0.13$ and $\alpha_{2,\mathrm{X}} = -2.40 \pm 0.19$ assuming $\omega = 3$, and $\alpha_{2,\mathrm{F606W}} = -1.96 \pm 0.07$ and $\alpha_{2,\mathrm{X}} = -2.23 \pm 0.15$ when $\omega = 10$. The optical and X-ray light curves and our best fits in both cases are shown in Figure 3.

We also fitted the decline using a single power law before 8.5 d and another after 26.5 d, ignoring the points in the vicinity of the break itself. The r' band light curve contains at least one smooth 'bump' feature, possibly two depending on t_j (we discuss the nature of the bump in Section 4.1). These may disturb the optical broken power-law fits; the reduced χ^2 values of these fits are rather high, although the small errors also contribute to this. The result is $\alpha_{2,\mathrm{F606W}} = -1.94 \pm 0.13$, nearly exactly coinciding with the $\omega = 10$ case but with a $\sim 2.5\sigma$ difference to $\omega = 3$. Repeating this in the X-ray results in $\alpha_{2,\mathrm{X}} = -2.20 \pm 0.13$, which is also almost identical to the $\omega = 10$ case. A simultaneous single power law fit to both post-break light curves results in $\alpha_2 = -2.01 \pm 0.09$.

Table 5. Parameters of the best smooth broken power law fits to the GRB 160625B light curves and of the single power law (SPL) fits to the early and late decline, ignoring the bump(s) between 8.5 and 26.5 d.

Parameter	$\omega = 3$	$\omega = 10$	SPL
$t_{j,\mathrm{F606W}}$	24 ± 3 d	17 ± 2 d	17 ± 4 d
$\alpha_{1,\mathrm{F606W}}$	-0.96 ± 0.01	-0.96 ± 0.01	-0.97 ± 0.01
$\alpha_{2,\mathrm{F606W}}$	-2.27 ± 0.13	-1.96 ± 0.07	-1.94 ± 0.13
Reduced χ^2	5.5	4.4	1.8
$t_{j,\mathrm{X}}$	27 ± 5 d	22 ± 4 d	22 ± 5 d
$\alpha_{1,\mathrm{X}}$	-1.24 ± 0.02	-1.24 ± 0.02	-1.25 ± 0.03
$\alpha_{2,\mathrm{X}}$	-2.40 ± 0.19	-2.23 ± 0.15	-2.20 ± 0.13
Reduced χ^2	0.91	0.81	0.84

Assuming an achromatic break, we determined t_j by taking the weighted average of $t_{j,\mathrm{F606W}}$ and $t_{j,\mathrm{X}}$. In the $\omega = 10$ case, the result is $t_j = 19 \pm 2$ d. Assuming an instantaneous break (corresponding to $\omega = \infty$) between the single power law fits, the resulting jet break times are consistent, $t_{j,\mathrm{F606W}} = 17 \pm 4$ d and $t_{j,\mathrm{X}} = 22 \pm 5$ d, and the weighted average $t_j = 19 \pm 3$ d. In the $\omega = 3$ case, we obtained $t_j = 25 \pm 3$ d.

For the radio light-curve of GRB 160625B, we combined flux measurements from Alexander et al. (2017) and Troja et al. (2017) with our own data. At 58.3 d and 209.0 d we have observations at 6.1 GHz; we therefore obtained flux densities at 6.1 GHz by power-law interpolation between 5 and 7.1 GHz literature values at 22.5 and 48.4 d. We also scaled the 7.4 GHz flux at 31.34 d assuming the same power law as at 22.5 d. Points earlier than 22.5 d were ignored in the analysis of the late afterglow due to the influence of the reverse shock (Alexander et al. 2017). The resulting best fit for the late-time light curve is $\alpha_{6.1\mathrm{GHz}} = -1.08 \pm 0.11$ as shown in Figure 3.

Additionally, we used the BOXFIT v.2 afterglow fitting code (van Eerten et al. 2012), based on the Afterglow Library[10], to fit the light curve. The library of models itself was constructed using the relativistic hydrodynamics code RAM (Zhang & MacFadyen 2006). BOXFIT then uses a downhill simplex method with simulated annealing to find the best fit, interpolating between these models. We omitted the pre-break radio points due to the influence of the reverse shock in the early light curve, and all the radio points below 5 GHz due to possible strong Milky Way scintillation (Alexan-

[10] http://cosmo.nyu.edu/afterglowlibrary/index.html

Table 6. Best-fit physical parameters of the best BOXFIT fits to GRB 160625B at three different values of the participation fraction ξ.

Parameter	$\xi = 1$	$\xi = 0.1$	$\xi = 0.01$
p	2.30	2.05	2.05
$E_{\rm K,iso}$ (erg)	1.8×10^{54}	1.4×10^{54}	1.3×10^{55}
ϵ_e	0.13	0.25	0.024
ϵ_B	0.030	3.0×10^{-4}	5.8×10^{-5}
n (cm^{-3})	1.1×10^{-5}	0.18	0.96
θ_j (rad)	0.059	0.14	0.13
θ_j (deg)	3.4	7.8	7.2
θ_{obs} (rad)	0.012	1.1×10^{-3}	1.1×10^{-3}
θ_{obs} (deg)	0.69	0.07	0.06
$E_{\rm tot}$ (erg)	8.3×10^{51}	4.1×10^{52}	1.3×10^{53}
η	0.62	0.68	0.19
χ^2/d.o.f	8.6	4.6	4.5

der et al. 2017). We also included the ultraviolet to near-infrared frequency data from Troja et al. (2017). We assumed an ISM-like CBM (the light curve rules out a wind-type CBM; see Section 4.2.1) and performed the fit with three different values of the participation fraction ξ, i.e. the fraction of electrons accelerated by the shock into a non-thermal power-law distribution. Simulations indicate this value can be as low as 0.01 (Sironi & Spitkovsky 2011; Sironi et al. 2013; Warren et al. 2018); we used fixed values of 1 (commonly assumed in the literature), 0.1 and 0.01. All other model parameters were allowed to vary within the full range allowed by BOXFIT. The resulting best-fit parameters are summarized in Table 6. Taking the isotropic-equivalent γ-ray energy $E_{\rm iso} = 3.0 \times 10^{54}$ erg (with the fluence from Svinkin et al. 2016), we also calculate the geometry-corrected total energy and the efficiency $\eta = E_{\rm iso}/(E_{\rm K,iso} + E_{\rm iso})$ for the conversion of kinetic energy to γ-rays. These fits, however, fail to reproduce the measured power law slope of $\alpha_{\rm 6.1GHz} = -1.08 \pm 0.11$, instead predicting a break in the radio light curve around ~ 100 d (associated with the passage of ν_m through this band). See Figure 4 for our best BOXFIT light curve fits. For clarity, we plot the U, F606W and H bands, covering the optical/infrared behavior from early to late times, but omit the other optical/infrared bands, which exhibit very similar behavior (see Troja et al. 2017). While the late-time 6.1 GHz light curve can be reproduced slightly better at low ξ values, the fit at higher frequencies or earlier times is still somewhat worse; we show 22 GHz as an example.

As some optical and X-ray observations are nearly contemporaneous, we can construct the spectral energy distribution (SED) of GRB 160625B. Figure 5 shows the SED at four epochs around or after the break, along

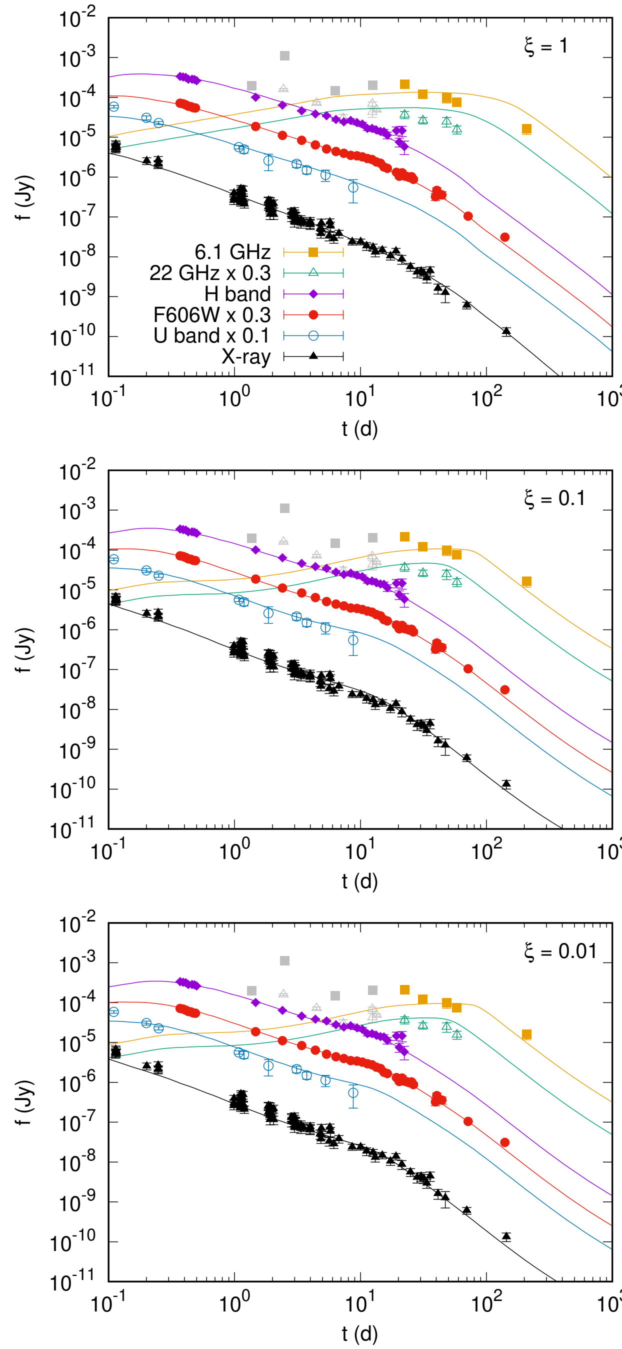

Figure 4. Observed X-ray, optical (U, F606W and H bands shown here) and interpolated 6.1 and 22 GHz light curves of the afterglow of GRB 160625B (points), and the best fits given by BOXFIT (lines) at indicated participation fraction ξ. The shape of the radio light curve is not well reproduced by any of the fits. Data denoted by grey points are ignored in the fitting (see text).

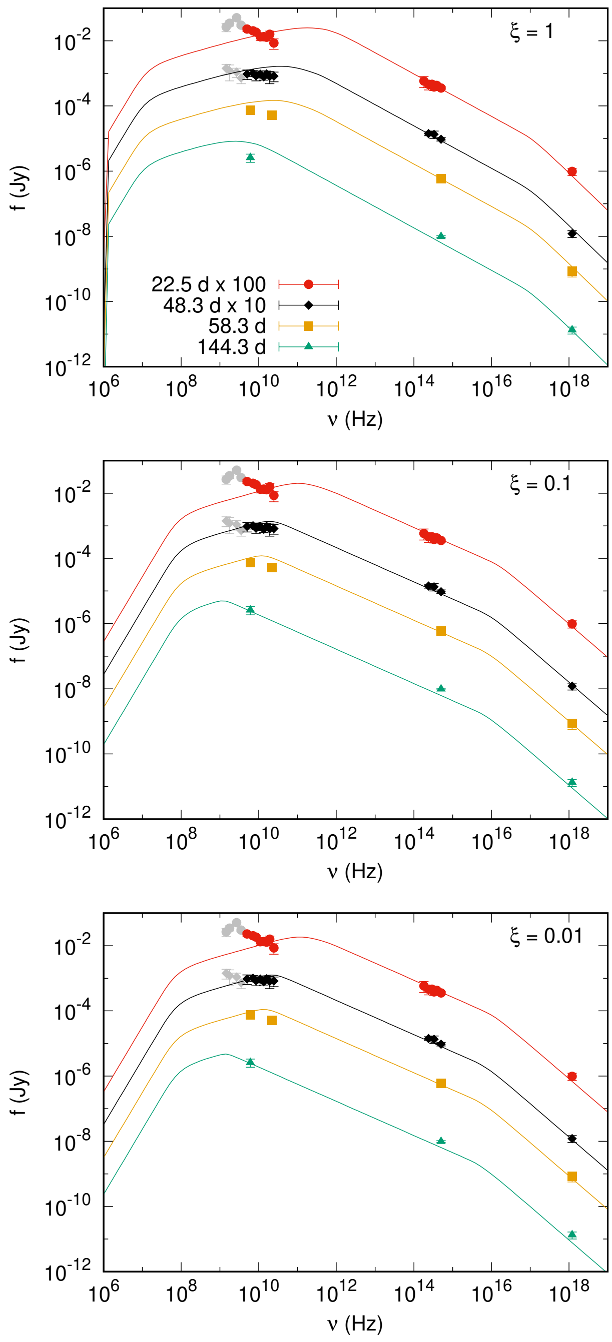

Figure 5. Observed spectral energy distribution of GRB 160625B (points) at late times, interpolated as necessary to the indicated dates, and the best fits given by BOXFIT (lines) at indicated participation fraction ξ, using an constant CBM density profile. Data denoted by grey points are ignored in the fitting (see text).

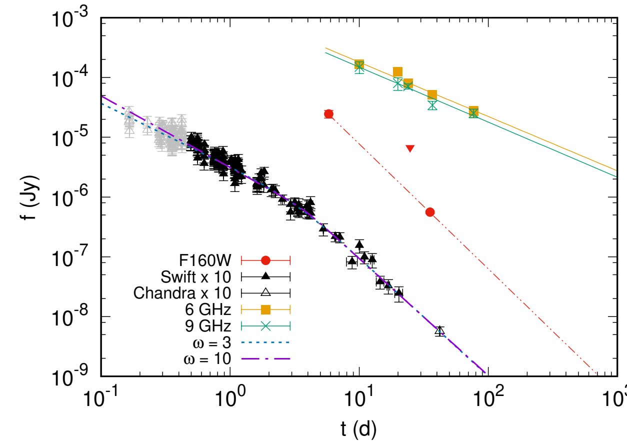

Figure 6. Observed F160W (extinction-corrected), X-ray and interpolated 6 and 9 GHz light curves of the afterglow of GRB 160509A (points) and our power law fits including the broken power laws described by Eq. 1 (lines). The red triangle is the upper limit of the F160W flux at 24.8 d. X-ray flux densities from *Swift*/XRT (solid triangles) and *Chandra*/ACIS-S (open triangles) are reported at 5 keV. Both choices of ω fit the late light curve equally well. The early light curve exhibits a shallower decay and another break, and thus points before 4×10^4 s (grey) are ignored.

with spectra produced by BOXFIT at these epochs. The power-law slope of the SED, β, between the optical (r) and X-ray (5 keV) bands, steepens slightly over time, from -0.79 ± 0.02 between 3 and 10 d to -0.86 ± 0.04 at 141 d. This is steeper than -0.65, expected from $p \approx 2.3$ implied by the early optical and X-ray light curves (see Section 4.2.1) for $\nu < \nu_c$, but shallower than -1.15, which is expected for $\nu > \nu_c$. Alexander et al. (2017) obtain an early X-ray spectral slope similar to this, $\beta_X = -0.86^{+0.09}_{-0.10}$, and explain this as ν_c being located just below the X-ray band. However, according to the UKSSDC *Swift* Burst Analyser[11] the X-ray photon index Γ_X (and thus the spectral slope in X-ray) does not significantly evolve over the first 30 d but stays around ~ 1.8, after which the spectrum seems to flatten to $\Gamma_X \sim 1.1$. This feature may not be real, though, as the Burst Analyzer light curve deviates much more from a clean power law when this is used in flux calculation – thus we assume a constant Γ_X[12]. If ν_c was initially just below X-ray and changed as $\nu_c \propto t^{-1/2}$, one would expect the spectrum to instead steepen over time to its $\nu \gg \nu_c$ value. We discuss this evolution further in Section 4.2.1.

3.2. *GRB 160509A*

It was noted in Laskar et al. (2016) that the host galaxy of GRB 160509A contributes substantially to the

[11] http://www.swift.ac.uk/burst_analyser/00020667/

[12] The post-break X-ray slope would not change by changing Γ_X at the latest *Swift* points, as *Chandra* points would be affected equally – but $t_{j,X}$ could be delayed.

optical and infrared photometry, and that the event occurred behind a significant amount of extinction in the host galaxy. In order to estimate the host galaxy extinction along the line of sight to the GRB, we removed the foreground Galactic reddening of $E(B-V) = 0.2519$ mag (Schlafly & Finkbeiner 2011) using the Cardelli et al. (1989) law, and assumed a $f_\nu \propto \nu^\beta$ SED, where $\beta = -0.6$ (consistent with $\nu < \nu_c$ and $p \approx 2.2$, determined based on the X-ray spectrum and light curve by Laskar et al. 2016). For the host, we assume the Pei (1992) extinction law for the Small Magellanic Cloud (SMC), as both Kann et al. (2006) and Schady et al. (2012) found the extinction curve in the SMC consistent with their samples. We fitted the observed optical-infrared SED simultaneously at two epochs, corrected using this extinction curve, to find the required extinction correction to match $\beta = -0.6$. The GRB flux in the g' band at 1 d was estimated by subtracting the observed flux at 28 d ($g' = 25.39 \pm 0.12$; Laskar et al. 2016) from the flux at 1.0 d ($g' = 25.03 \pm 0.15$; Cenko et al. 2016). The host is assumed to dominate at 28 d due to the flatness of the light curve even after the X-ray break. In the J band, we subtracted the flux of the host galaxy measured in the *HST* F110W filter (using a 1 arcsec aperture) from the flux at 1.2 d ($J \approx 19.7$; Tanvir et al. 2016). The r' band was not included in the SED, as the late and early fluxes are consistent within 1σ (Cenko et al. 2016; Laskar et al. 2016). Our F110W and F160W observations at 35.3 d made up the other epoch to be fitted simultaneously. The resulting host extinction is $A_V = 2.8 \pm 0.1$ mag in the rest-frame (this is somewhat lower than the result obtained by Laskar et al. 2016, using an afterglow model fit where the host flux was a free parameter). Using the Pei (1992) law, the extinction correction in F160W (approximately i-band in the rest frame) is thus 1.5 mag. In the Milky Way, the adopted $N_{\rm H,int} = 1.52 \times 10^{22}$ cm^{-2} would correspond to $A_V \approx 6.9$ mag (Güver & Özel 2009), suggesting a low A_V/N_H ratio for Milky Way standards but higher than that of most GRB hosts. This ratio is consistent with the A_V vs. N_H/A_V relation in Krühler et al. (2011). As in the case of GRB 160625B, we combined our *Chandra* data of GRB 160509A with the data from the *Swift*/XRT light curve repository converted to 5 keV flux densities.

The CIRCE H-band fluxes were converted to the narrower F160W filter assuming $\beta = -0.6$. The F160W and X-ray data and our power-law fits are presented in Figure 6, and the parameters of the fits are listed in Table 7. For our power law fits we ignore the data points before ~ 0.5 d (4×10^4 s), as the early X-ray light curve may contain a plateau and/or a flare; see Figure 6. In this case the smooth- and sharp-break scenarios give similar results: the best fit for the post-break decline for $\omega = 3$ is $\alpha_{2,\rm X} = -1.98 \pm 0.10$ and for $\omega = 10$, $\alpha_{2,\rm X} = -1.96 \pm 0.09$. The jet-break times, 3.2 ± 0.9 d and 3.7 ± 0.8 d, respectively, are consistent with each other as well.

Table 7. Parameters of the best smooth broken power law fits to the GRB 160509A X-ray light curve.

Parameter	$\omega = 3$	$\omega = 10$
$t_{j,\rm X}$	3.2 ± 0.9 d	3.7 ± 0.8 d
$\alpha_{1,\rm X}$	-1.06 ± 0.10	-1.20 ± 0.06
$\alpha_{2,\rm X}$	-1.98 ± 0.10	-1.96 ± 0.09
Reduced χ^2	0.84	0.85

In the radio, we obtained the fluxes at 6 and 9 GHz at the epochs earlier than 79.9 d by power-law interpolation between observed fluxes – our measurements at 36.9 d and those published in Laskar et al. (2016) at earlier times. We then fitted a single power law to the points where the reverse shock should no longer dominate the radio flux (i.e. ≥ 10 days; Laskar et al. 2016). The resulting decline slopes are $\alpha_{\rm 6GHz} = -0.91 \pm 0.11$ and $\alpha_{\rm 9GHz} = -0.92 \pm 0.13$. Since the reverse shock may still be contributing a non-negligible fraction of the flux at 10 d, we also performed the fit without this epoch. The results are consistent but less constraining: $\alpha_{\rm 6GHz} = -1.07 \pm 0.18$ and $\alpha_{\rm 9GHz} = -0.92 \pm 0.21$. The slopes at other frequencies between 5 and 16 GHz, fitted from 10 to 20 d, are all consistent with these, ranging from -0.80 ± 0.10 (7.4 GHz) to -1.02 ± 0.04 (8.5 GHz). In F160W and/or H, we only have two points and an upper limit; therefore we simply measure the decline assuming a single power law. As the first point at 5.8 d is after the jet break time we obtained from the X-ray fit, there should be no significant deviation from a single power law. The measured decline is $\alpha_{2,\rm F160W} = -2.09 \pm 0.10$, consistent within 1σ with the X-ray decline.

Using BOXFIT, we again fitted the light curve at three different values of ξ: 1, 0.1 and 0.01. As with the power-law fits, the X-ray points before 0.6 d were ignored, since BOXFIT cannot accommodate continuous energy injection. Radio points with a significant reverse shock contribution were also ignored (i.e. < 10 d; at frequencies < 5 GHz also 10.03 d; see Laskar et al. 2016). We ran BOXFIT with the boosted-frame wind-like CBM model (with both strong and medium boost) and a lab-frame model with ISM-like CBM, as the lack of optical data makes it difficult to distinguish between different CBM profiles (although the ISM scenario is tentatively favored by Laskar et al. 2016). However, as shown in Figure 7, our fits in a wind CBM do not reproduce the jet break

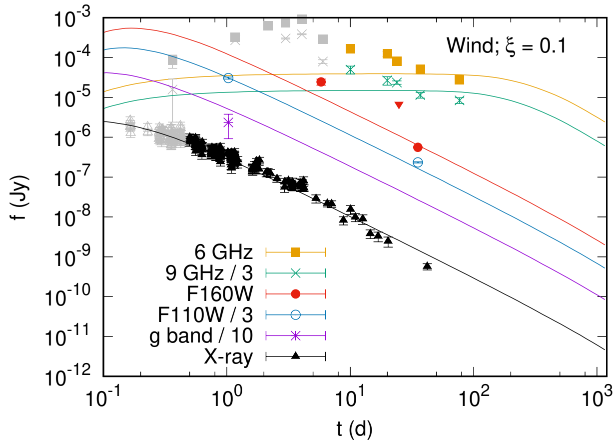

Figure 7. Observed X-ray and optical/infrared light curves and the interpolated 6 and 9 GHz light curves of the afterglow of GRB 160509A (points), and the best fit given by BOXFIT (lines) using a wind-type CBM density profile and $\xi = 0.1$. The observed X-ray break is not reproduced (and indeed no break is seen even much later), and therefore a wind-type CBM is not considered further. Fits using $\xi = 1$ and $\xi = 0.01$ produce a similar light curve. Data denoted by grey points are ignored in the fitting (see text).

clearly detected in the X-ray light curve. Even with the parameters in Laskar et al. (2016), the break only appears at ~ 100 d and the X-ray fit is much worse than with an ISM-type CBM. Thus the analytical model and BOXFIT seem to disagree on how the jet behaves in a wind-type CBM, and we concentrate on the ISM scenario. The best ISM fits are shown in Figure 8; Figure 9 shows the SED at three post-break epochs along with specra produced by BOXFIT at these epochs. Our resulting best-fit parameters are summarized in Table 8. These fits (including the wind fits) again fail to match the observed shape of the radio light curve, although the amplitude of the flux can be reproduced at some epochs.

4. DISCUSSION

4.1. *The shape of the break*

In the X-ray, we find little difference in the reduced χ^2 values of the fits between a sharp and a smooth break for GRB160625B. In the optical, however, fixing $\omega = 3$ results in a visible and significant residual of 4.2σ at 140.2 d, while fixing $\omega = 10$ results in a residual of 1.5σ. The reduced χ^2 of the latter fit is also slightly smaller. In the optical light curve, one can see either one slight bump or two, depending on the break time. These deviations from a perfect power law may disturb the fit and cause the high χ^2 values, which suggests that one should also try only using the post-break points. Simply fitting a single power law to the points after 26.5 d results in consistency with the $\omega = 10$ case. We thus

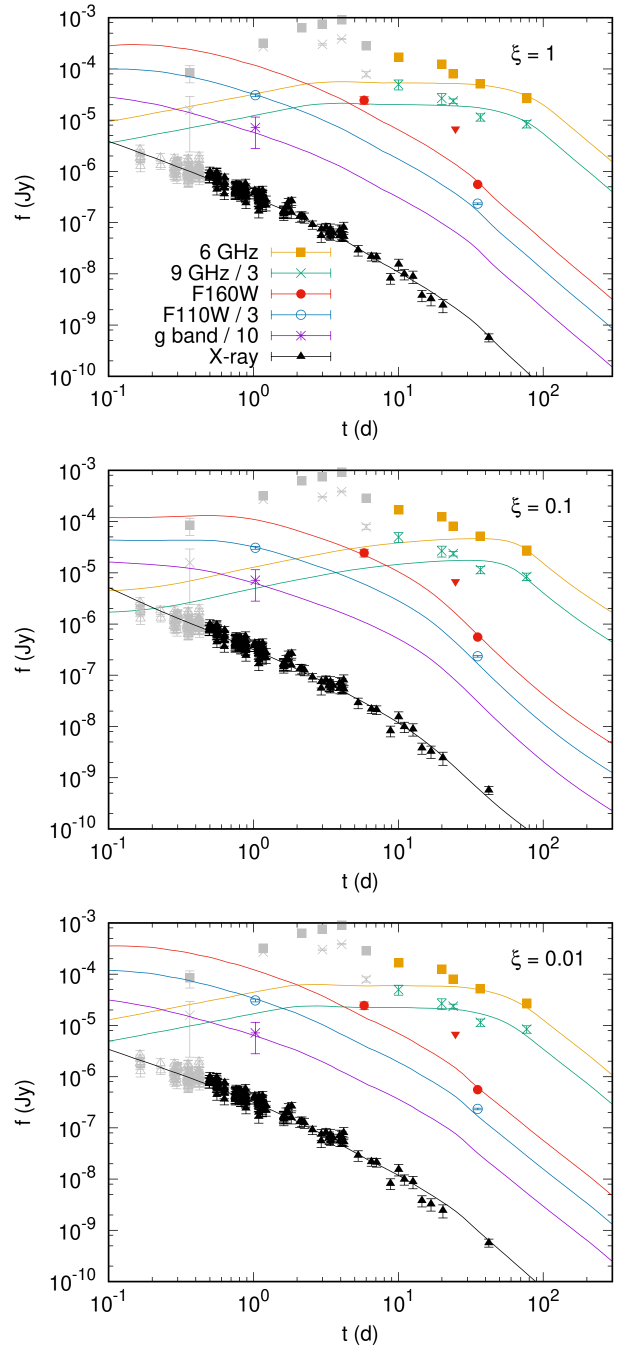

Figure 8. Observed X-ray and optical/infrared light curves and the interpolated 6 and 9 GHz light curves of the afterglow of GRB 160509A (points), and the best fits given by BOXFIT (lines) at indicated participation fraction ξ, using an ISM-type CBM density profile. The radio light curve shape is again not well reproduced by the fits. Data denoted by grey points are ignored in the fitting (see text).

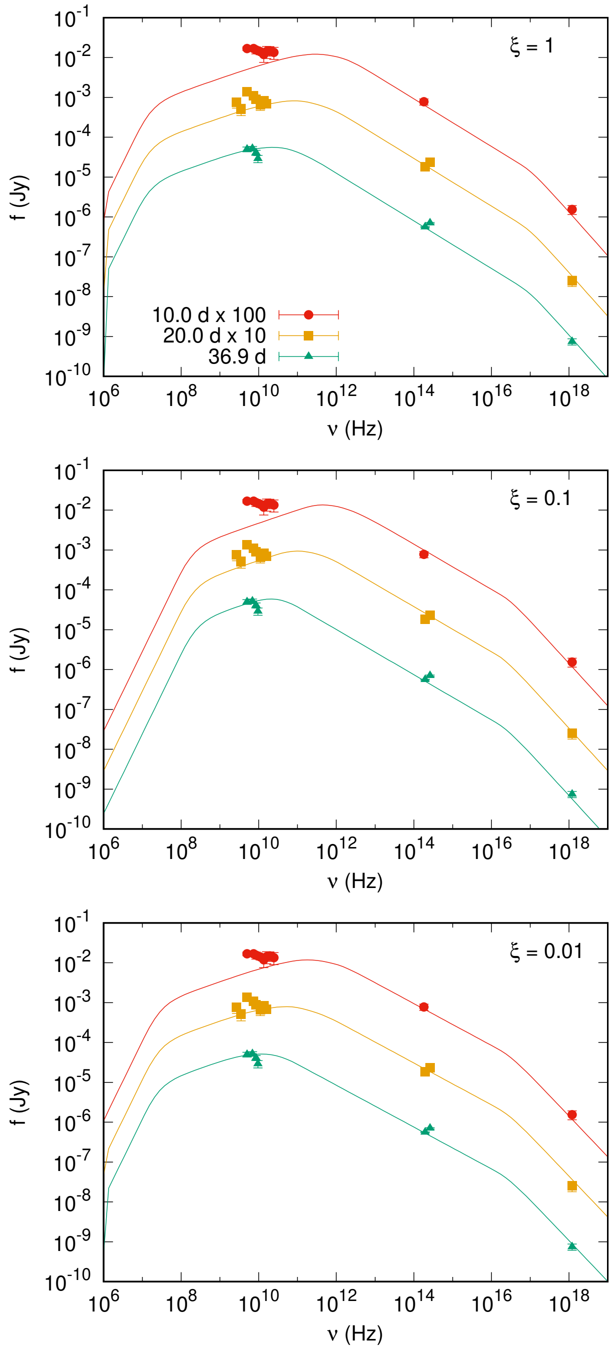

Figure 9. Observed spectral energy distribution of GRB 160509A (points) at late times, interpolated as necessary to the indicated dates, and the best fits given by BOXFIT (lines) at indicated participation fraction ξ, using an ISM-type CBM density profile.

conclude that while both values of ω remain plausible, a sharp break with $\omega = 10$ is more likely. A sharp break also implies a small viewing angle θ_{obs} (Ryan et al. 2015), which is compatible with the BOXFIT results for this burst.

Table 8. Best-fit physical parameters of the best BOXFIT fits to GRB 160509A at three different values of the participation fraction ξ.

Parameter	$\xi = 1$	$\xi = 0.1$	$\xi = 0.01$
p	2.29	2.13	2.05
$E_{\rm K,iso}$ (erg)	8.5×10^{53}	3.8×10^{53}	3.8×10^{55}
ϵ_e	0.19	0.45	5.7×10^{-3}
ϵ_B	0.015	1.7×10^{-5}	5.8×10^{-4}
n (cm^{-3})	2.1×10^{-5}	18.1	6.1×10^{-3}
θ_j (rad)	0.046	0.20	0.045
θ_j (deg)	2.6	11.5	2.6
θ_{obs} (rad)	0.026	0.12	0.027
θ_{obs} (deg)	1.5	7.0	1.5
$E_{\rm tot}$ (erg)	1.7×10^{51}	2.5×10^{52}	3.9×10^{52}
η	0.50	0.69	0.02
χ^2/d.o.f	1.8	1.9	1.8

The post-jet-break decline of GRB 160625B has been previously estimated to be $f_\nu \propto t^{\alpha_2}$, where generally $\alpha_2 \sim -2.3$ and its error roughly 0.5 (Alexander et al. 2017; Fraija et al. 2017; Lü et al. 2017). These estimates are largely consistent with both sharp and smooth breaks (and with our results listed in Table 5). However, all of these results are based on observations no later than $\sim$ 50 d from the burst ($\sim 2.5 \times t_j$, compared to our latest observations at $\sim 7 \times t_j$), and their post-break fluxes mostly include relatively large uncertainties. In addition, Troja et al. (2017) obtained a more precise post-break slope of $\alpha_2 = -2.57 \pm 0.04$ and Strausbaugh et al. (2018) obtained $\alpha_{2,\rm optical} \approx 1.6$ and $\alpha_{2,\rm X} = -2.06 \pm 0.22$, but their optical slope is inconsistent with our later-time optical data in both cases.

Troja et al. (2017) placed their estimate of the jet break at 14 d, during the 'bump' in the light curve between $\sim$ 8 d and $\sim$ 16 d. Using the same data, Strausbaugh et al. (2018) suggested a break at 12.6 d at the peak of the bump, which they took as brightening of the jet toward its edges. However, our later-time data require a later break and a steeper α_2, leading us to suggest the bump may still be due to angular brightness differences or perhaps the result of density fluctuations in the CBM, but not necessarily a sign of a bright edge – and seemingly not simultaneous with a true jet break. The bump is not seen in the X-rays, which is also consistent with a density fluctuation, as the flux above ν_c is insensitive to ambient density (Kumar 2000). Strausbaugh et al. (2018) also suggest that a slowly changing spectral slope in the optical bands indicates a gradual cooling transition instead of a ν_c break in the spectrum, and that the optical spectrum eventually becomes consistent with $\beta \sim -1.1$, i.e. the slope above ν_c, which would disfavor a CBM density fluctuation because of this insensitivity. We, however, measure $\beta = -0.86 \pm 0.04$ between F606W and 5 keV at 141 d, suggesting that ν_c is still above optical frequencies but below X-ray at this time. Thus we cannot rule out either scenario for the bump, but we can place the jet break at an epoch after the bump.

In the case of GRB 160509A, the χ^2 values of the fits with different ω are close to equal and the post-break slopes are in agreement. A higher θ_{obs} results in a softer break (Ryan et al. 2015), so in this case, considering that $\theta_{obs} \sim 0.6\theta_j$ (from BOXFIT), one would expect the break to be softer than for GRB 160625B where θ_{obs} is much smaller or close to zero. One can attempt to resolve this by finding inconsistencies in estimates of p based on the pre-break light curve and spectrum. The X-ray spectrum, with a slope of $\beta = -1.07 \pm 0.04$, is consistent with $p \approx 2.2$ and with ν_c being below the X-ray band (Laskar et al. 2016). As a result, we can use $\alpha = (2-3p)/4$ independent of the CBM distribution (Granot & Sari 2002); in the case of $\omega = 3$ we obtain $p = 2.08 \pm 0.14$ and for $\omega = 10$, $p = 2.27 \pm 0.08$. While the former is closer to the measured post-break decline, both values are consistent with 2.2.

4.2. *Physical implications*

4.2.1. *GRB 160625B*

Based on the well-constrained pre-break light curve of the afterglow of GRB 160625B, one can estimate the electron energy distribution index p: below the cooling frequency ν_c, in the case of a wind-like CBM, $\alpha_{\rm wind} = (1-3p)/4$, while for a constant-density CBM similar to the interstellar medium (ISM), $\alpha_{\rm ISM} = 3(1-p)/4$ (Granot & Sari 2002). Thus, in the optical, one obtains $p = 1.63 \pm 0.02$ in the wind case and $p = 2.29 \pm 0.02$ in the ISM case. Above ν_c, in both cases $\alpha = (2-3p)/4$. Comparing the optical and X-ray spectra and fluxes Alexander et al. (2017) argue that ν_c lies below the X-ray frequencies after $\sim 1.2 \times 10^4$ s, and thus the early X-ray light curve gives us $p = 2.29 \pm 0.06$. This is also consistent with the spectrum below the X-ray frequencies (Alexander et al. 2017), and thus, as the p values in the wind scenario are mutually inconsistent, an ISM-like density profile is favored. Fraija et al. (2017) infer a transition from wind-like to ISM-like CBM at ~ 8000 s.

When only taking into account the relativistic visible-edge effect (Mészáros & Rees 1999), the slope of the decline is expected to steepen in the jet break by a factor of $t^{-3/4}$ in a constant-density CBM. In the $\omega = 10$ case, the difference between the pre- and post-break power laws is $\Delta\alpha_{\rm F606W} = -1.00 \pm 0.08$ in the optical and $\Delta\alpha_{\rm X} = -0.99 \pm 0.16$ in the X-ray. Thus a $t^{-3/4}$ factor can be ruled out in the optical at a $> 3\sigma$ level (although in the X-ray, only at a $\sim 1.5\sigma$ level). The difference is larger in the $\omega = 3$ case ($> 4\sigma$ and $> 2\sigma$ respectively), and therefore a simple edge effect is inconsistent with our observations regardless of whether the break is sharp or smooth (the $t^{-1/2}$ factor from a wind-like CBM is, of course, even less plausible).

If one assumes a smooth break ($\omega = 3$), both the optical and X-ray post-break decline rates are consistent with the form $f_\nu \propto t^{-p}$, for $p \approx 2.3$, as expected from exponential lateral expansion (Rhoads 1999; Sari et al. 1999). At first glance, the favored sharp-break scenario seems to make GRB 160625B inconsistent with a $f_\nu \propto t^{-p}$ decline in the optical band (the X-ray slope is still consistent with it) and would seem to require another physical mechanism. One explanation could be that the true jet break is due to a combination of the visible-edge effect and more limited lateral expansion. The steepening in both bands is a factor of t^{-1}, steeper than the $t^{-3/4}$ expected from the edge effect (Mészáros & Rees 1999; Panaitescu & Mészáros 1999), and the resulting α_2 values are only consistent within 2σ, while the full exponential lateral expansion scenario described by Rhoads (1999) should result in identical slopes. In some numerical simulations, lateral expansion has been found to initially involve only the outer layer of the jet carrying a fraction of its energy, and the bulk of the material remains unaffected for some time (van Eerten & MacFadyen 2012), while the results of Rhoads (1999) require the assumption that the entire jet expands at the speed of sound. On the other hand, completely ignoring the lateral expansion was found to result in insufficient steepening across the jet break. This scenario seems consistent with our results.

A complication was noted by Gompertz et al. (2018), who find that using different synchrotron relations to estimate p (such as using the spectral index or the pre- or post-break decline) typically results in different estimates, with an intrinsic scatter on the value of p of 0.25 ± 0.04 (we will denote this as σ_p). They argue this is probably caused by emission from GRB afterglows not behaving exactly as the rather simplified analytical models predict[13]. Taking this scatter into account, both $\alpha_{2,\rm F606W}$ and $\alpha_{2,\rm X}$ in the $\omega = 10$ case (or simply using only the > 26.5 d points and a single power law) are in fact consistent within $\approx 1\sigma_p$ with $f_\nu \propto t^{-p}$. Thus lateral expansion at the speed of sound can still account for

[13] We note that the inconsistency between p values derived from the optical and X-ray pre-break slopes assuming a wind-type CBM is $> 2\sigma_p$, so an ISM-like density profile is still favored.

the observed late-time decline. Using closure relations for both the light curve and the spectrum, Gompertz et al. (2018) found a best fit of $p = 2.06 \pm 0.13$ for GRB 160625B, which is consistent with our results in both bands within σ_p. In any case, for this burst some form of lateral expansion is required, and the edge effect alone is insufficient.

We can also attempt to use the results from BOXFIT to determine if the magnetar spin-down power source is consistent with the GRB. The rotational energy that can be extracted from a millisecond magnetar is (Lü & Zhang 2014; Kumar & Zhang 2015)

$$E_{\rm rot} \approx 2 \times 10^{52} \text{ erg } \frac{M}{1.4\ M_\odot}\left(\frac{R}{10\text{ km}}\right)^2\left(\frac{P_0}{1\text{ ms}}\right)^{-2}, \quad (2)$$

where M is the mass, R the radius and P_0 the initial spin period of the newborn magnetar. Metzger et al. (2015) placed a limit of $\sim 1 \times 10^{53}$ erg on the maximum energy of a newborn magnetar in extreme circumstances (in terms of mass and spin period). Therefore the energy requirements of all the fits from BOXFIT may technically be achievable with the magnetar model, but with the (more realistic) low ξ values the required energy approaches or exceeds even this maximum limit. The exceptionally high $E_{\rm iso}$ can be due to a relatively narrow jet and a lower explosion energy instead, but this requires a high ξ that is inconsistent with simulations by Sironi & Spitkovsky (2011) and Warren et al. (2018) – the best fit at $\xi = 1$ also results in an extremely low density more typical to intergalactic environments. We do point out a caveat that the parameters of the best fits show a non-monotonic dependence on ξ, with notable degeneracy between parameters.

We have attempted to use BOXFIT to estimate errors for the best-fit parameters as well. However, as a result of what seems to be a bug in the error estimation routine of BOXFIT (G. Ryan and H. van Eerten, private communication), some of the errors are clearly incorrect and, therefore, we have not included errors in our Table 6. This mostly manifests as error limits that either do not include the best fit or where the best-fit value of a parameter is always the lower limit as well[14]. We also note that, as the shape of the radio light curve is not well reproduced in any of our fits, error limits could be misleading in any case. As a consistency check for the rest of the code, we have run BOXFIT using the Alexander et al. (2017) forward shock parameters, which are similar to our $\xi = 1$ results. The output light curves and spectra are similar to the analytical ones and reproduce the early behavior of the afterglow well, although post-break fluxes are somewhat under-predicted.

We also note that the 6.1 GHz light curve of GRB 160625B is not successfully reproduced by BOXFIT, and the jet model struggles to explain the late slope of $\alpha_{\rm 6.1GHz} = -1.08 \pm 0.11$ and the lack of an observed jet break. At low ξ values, the BOXFIT fit is somewhat better, but only if one ignores the 22.5 d point, where a low-frequency scattering event by an intervening screen, suggested by Alexander et al. (2017), may contribute to the flux. The radio SED shows a peak centered at 3 GHz between 12 and 22 d, which then disappears. Even so, the fit at 22 GHz is worse at all ξ values. At 48 d, the radio SED is consistent with being entirely flat, which is only plausible in the standard model around a very smooth ν_m break. While the low ξ fits do place the ν_m passage at roughly this time, the peak in the BOXFIT spectrum is too sharp, and in earlier spectra the lowest frequencies must then be brightened by a factor of ten or so by the proposed scattering. The shape may instead be altered by another emission source contributing to the spectrum (see below).

Theoretically expected post-break values in the slow-cooling scenario ($\nu_m < \nu_c$) are $-p$ or $-1/3$, depending on which side of ν_m the band is located (Rhoads 1999). As the jet break is a geometric effect, we should see it in every band, but this is not the case: we can set a limit of $t_{j,\rm 6.1GHz} \gtrsim 10 \times t_{j,\rm F606W}$. The possibilities given by the standard jet model that are consistent with the slope are:

- Post-break, $\nu_c < \nu_m$, i.e. fast-cooling: $\alpha_{\rm 6.1GHz}$ is consistent with the expected decline of $\alpha_2 = -1$. However, the measured $\alpha_{1,\rm F606W} = -0.96 \pm 0.01$ does not match the *pre*-break decline expected at any frequency in this scenario.

- Pre-break, $\nu_m < 6.1$ GHz $< \nu_c$: $\alpha_{\rm 6.1GHz}$ is consistent with $p = 2.4$ and $\alpha = 3(1-p)/4 = -1.05$ (Granot & Sari 2002). However, the spectral index between radio and optical is -0.35 ± 0.03 at 22 d and -0.49 ± 0.01 at 140 d, which is intermediate between the indices expected above and below ν_m (respectively, $(1-p)/2 \approx -0.65$ and $1/3$) and thus implies that $\nu_m > 6.1$ GHz at 140 d, or that $p \approx 2.0$.

- A transition to a non-relativistic flow, $\nu_m < 6.1$ GHz $< \nu_c$: the expected slope is $(21 - 15p)/10$ (van der Horst 2007), resulting in $p = 2.12 \pm 0.08$,

[14] In other cases, such as the $\xi = 0.1$ case of GRB 160625B, the errors are *seemingly* reasonable ($p = 2.05 \pm 0.01$, $E_{\rm K,iso} = 1.4^{+1.2}_{-1.3} \times 10^{54}$ erg, $\epsilon_e = 0.25^{+0.10}_{-0.13}$, $\epsilon_B = 3.0^{+106.3}_{-2.0} \times 10^{-4}$, $n = 0.18^{+0.58}_{-0.15}$ cm^{-3}, $\theta_j = 0.14 \pm 0.03$ rad and $\theta_{obs} = 1.1^{+5.9}_{-1.1} \times 10^{-3}$ rad) and the relative ranges of each parameter comparable to those found by Alexander et al. (2017). These values thus give an indication of how well each parameter is constrained.

which is consistent with our estimate within σ_p. However, such a transition is not seen in the optical or X-ray bands.

The LGRB population has been observed to be comprised of a radio-quiet and a radio-loud population, where the radio-quiet GRBs are incompatible with a simple sensitivity effect and indicate an actual deficit in radio flux compared to theory (Hancock et al. 2013). Lloyd-Ronning et al. (2019) further argued that the two populations originate in different progenitor scenarios. This deficit in radio flux implies some mechanism that suppresses the expected synchrotron emission at radio frequencies. Since our findings indicate that the radio light curve of GRB 160625B (and GRB 160509A; see below) is incompatible with the higher frequencies, the source of the radio emission that we do see may not be the same as that of the optical and X-ray synchrotron emission. This seems to suggest that even in (at least) some radio-loud GRBs, the same mechanism may be in effect. Furthermore, if the radio emission is generated by another source, this source is not active in the radio-quiet GRBs for some reason. We have run the BOXFIT fitting code with $\xi = 1$ and all radio fluxes divided by ten to investigate if the standard model allows suppression of the radio flux simply through adjusting the parameters. The resulting best fit over-predicts all radio fluxes by at least a factor of a few at all times. This implies a caveat that, at least in some cases, including another, dominant radio source without an additional suppression mechanism may over-predict the radio flux. Another caveat with this is that, unless the second component is coupled to the 'main' source, getting a total radio flux compatible with one component may require fine-tuning. If such a mechanism is widespread, one would expect some GRBs to have radio fluxes unambiguously too high for the standard model, which, to our knowledge, has not been seen.

One explanation for the 'extra' radio source, with its lack of a jet break and the requirement of 6.1 GHz $> \nu_m$, could be a two-component jet, where a narrow jet core is surrounded by a cocoon with a lower Lorentz factor (Berger et al. 2003; Peng et al. 2005), resulting in a different source with different physical parameters dominating the radio emission, and thus a different break time and ν_m. This does not result in a deficit in radio synchrotron flux, only an inconsistency between the light curve shape and the standard model. For an on-axis or slightly off-axis burst ($\theta_{obs} < \theta_{j,\mathrm{narrow}}$), the wider component would not contribute significantly to the optical light curve if its kinetic energy is lower than that of the narrow component (Peng et al. 2005). This may also affect the required energy, but without robust modeling it is difficult to say whether the consistency with a magnetar energy source would change.

Strausbaugh et al. (2018) suggested a scenario where a very smooth cooling transition (i.e. not a normal spectral break) is moving through the optical and infrared frequencies, starting at early times, and the optical spectrum becomes consistent with $\nu > \nu_c$ by ~ 50 d. This would indicate a unique cooling behavior inconsistent with the standard expectations. The observed lack of evolution of the *Swift* spectra until 30 d implies that the X-ray spectral slope β_X is not the result of a ν_c break right below the X-ray frequencies, as this would require the spectrum to soften over time to its slope at $\nu \gg \nu_c$. Furthermore the optical-to-X-ray index is observed to gradually steepen and eventually become similar to β_X. This is qualitatively consistent with the reddening of the optical spectrum noted by Strausbaugh et al. (2018). In addition, β_X indicates a different p than the X-ray light curve; this agrees with the implication of Gompertz et al. (2018) that some physics is missing or simplified in the relevant closure relations. Another possible explanation is that a Klein-Nishina correction (Nakar et al. 2009) is needed above ν_c; this can result in $\beta = 3(1-p)/4$, which would imply $p \approx 2.1$. This harder spectrum is expected to dominate when the ϵ_e/ϵ_B ratio is high, which would fit the low-ξ BOXFIT results.

4.2.2. *GRB 160509A*

In the case of GRB 160509A, the change in X-ray decay slope across the break, $\Delta\alpha_{\mathrm{X}} = -0.75 \pm 0.11$ for a sharp break and $\Delta\alpha_{\mathrm{X}} = -0.92 \pm 0.15$ for a smooth break. Thus we cannot exclude the $t^{-3/4}$ factor expected from the edge effect alone in an ISM-like medium. The $t^{-1/2}$ factor expected in the case of a wind medium is inconsistent with the observations at a 2.3σ or 3σ level, depending on ω. However, when considering the intrinsic p scatter of $\sigma_p = 0.25$ (Gompertz et al. 2018), $\alpha_{2,\mathrm{X}}$ is also consistent with a $f_\nu \propto t^{-p}$ decline. Thus we cannot say conclusively whether lateral expansion is important in the jet of GRB 160509A, but it does not seem *necessary.* In the IR, the measured slope of $\alpha_{2,\mathrm{F160W}} = 2.09 \pm 0.10$ is marginally consistent (1.1σ) with $p \approx 2.2$, but a lack of pre-break data prevents us from determining $\Delta\alpha_{\mathrm{F160W}}$.

The decline of the afterglow in the radio after 10 d is about $f \propto t^{-0.9}$ at both 6 and 9 GHz (and consistent with this at other frequencies where fewer points are available). This is again inconsistent with the expected post-jet-break slope of $-p$ or $-1/3$ in the slow-cooling case, respectively above and below the characteristic synchrotron frequency ν_m (Rhoads 1999). As with GRB 160625B, we list the possibilities consistent with this decline, allowed by standard jet theory:

- Post-break, $\nu_c < \nu_m$, i.e. fast-cooling: $\alpha = -1$ is expected and consistent with $\alpha_{\rm radio}$, but this scenario is incompatible with the measured IR-to-X-ray spectral index -0.74 ± 0.09 at 35 d, as the expected index is $-p/2 \approx -1.1$ (a photon index consistent with this is indeed seen in the X-ray at earlier times according to the UKSSDC *Swift* Burst Analyser[15] – $< \beta_X >= 1.06 \pm 0.04$ between 1 and 10 d – indicating that ν_c is still between X-ray and optical frequencies and $\nu_c > \nu_m$ at 35 d).

- Pre-break, $\nu_m < 6$ GHz $< \nu_c$, ISM-like CBM: $\alpha_{\rm radio}$ is consistent with the expected decline ($\alpha = 3(1-p)/4 = -0.9$ assuming $p = 2.2$; Granot & Sari 2002), but the observed spectral index of -0.40 ± 0.01 between F160W and 9 GHz at 35 d implies $\nu_m > 9$ GHz.

- A transition to a non-relativistic flow, $\nu_m < 6$ GHz < 9 GHz $< \nu_c$: the expected slope is $(21 - 15p)/10$, resulting in $p = 2.01 \pm 0.08$ – again consistent with our estimate within σ_p. However, such a transition is not seen in the X-ray light curve, which continues to evolve consistently with a relativistic flow.

The best boxfit fit at $\xi = 1$ places a smooth, and thus off-axis, jet-break at a later time, around 35 d in all bands, in which case the radio light curve would include contamination from the reverse shock at early times, changing the decline slope (see Figure 8). This is because boxfit attempts to fit a model with a late break to $f_\nu \propto t^{-p}$ in order to match the radio light curve, which has no observed break. It is incompatible with the broken power-law fit with $t_j \sim 3.5$ d, though, and at lower, more realistic values of ξ the break is placed at an earlier time. This scenario is therefore not supported. Instead, for GRB 160509A we can place a lower limit of $t_{j,\rm radio} \gtrsim 20 \times t_{j,\rm X}$ based on the broken power-law fit. The situation in the radio frequencies is thus qualitatively very similar to that of GRB 160625B, and the same mechanisms may well be in effect.

We note that Kangas & Fruchter (2019) are, in fact, able to get a plausible fit to the GRB 160509A radio light curve using an analytical fit based on the standard model, but only if the light curve smoothly turns over to a t^{-p} decline immediately after the last radio epoch, which is suspicious as their sample contains several GRBs with no unambiguously observed radio breaks, and many cases where the standard model does not fit the radio light curve. We also note that as Laskar et al. (2016) showed, the radio SED seems to remain roughly flat after the reverse shock influence on the light curve fades (~ 20 d), which might again be caused by another emission component. As boxfit also disagrees with this analytical model, one or the other is in doubt. The issue will be addressed in more detail in the upcoming revised version of that paper.

A boxfit simulation using the FS parameters of the Laskar et al. (2016) analytical model agrees fairly well with the X-ray data and reproduces the rough magnitude of the radio light curve but not its shape (assuming some RS contribution not accounted for by boxfit), but over-predicts the IR flux by a factor of about 10. Their IR light curve does not include host subtraction, and they fit for extinction as another free parameter in their model. Our host subtraction allows us to estimate the extinction and true IR fluxes independently, and in light of this the Laskar et al. (2016) model becomes incompatible with the IR data. Thus our boxfit results provide a better reproduction of the light curve in the IR. However, again, the fit parameters show a non-monotonic dependence on ξ. As with GRB 160625B above, boxfit was clearly unable to produce meaningful error bars for the parameters in some cases, and these are not included in Table 8[16] – and, as the radio light curve is again problematic for the fit, would be misleading in any case.

Keeping in mind the caveats associated with our best boxfit fits, we can use them to estimate the energy requirements. The geometry-corrected jet energy 1.8×10^{51} erg at $\xi = 1$ is well below the maximum rotational energy of a millisecond magnetar (see Section 4.2.1) Once again, we deem the lower ξ values more realistic based on simulations (Sironi & Spitkovsky 2011; Warren et al. 2018) and the fact that $\xi = 1$ results in an extremely low density. Low ξ values require energies around $\sim 3 \times 10^{52}$ erg, which again strains the magnetar spin-down model but does not rule it out. Thus GRB 160509A also seems compatible with a magnetar power source.

For both GRBs considered here (Tables 6 and 8), but especially for GRB 160509A, the efficiency η of the prompt γ-ray emission depends on the value of ξ used in the fitting, but not monotonically: with $\xi = 0.01$ one obtains a much lower value for η than otherwise. In both cases, the difference in χ^2 between the $\xi = 0.1$ and $\xi =$

[15] http://www.swift.ac.uk/burst_analyser/00020607/

[16] Again, the ranges of each parameter at $\xi = 0.1$, which are large but not obviously incorrect, may provide some indication of how well each parameter is constrained: ($p = 2.13^{+0.02}_{-0.01}$, $E_{\rm K,iso} = 3.8^{+24.8}_{-3.4} \times 10^{53}$ erg, $\epsilon_e = 0.45^{+0.31}_{-0.20}$, $\epsilon_B = 1.7^{+2.7}_{-0.7} \times 10^{-5}$, $n = 18^{+1530}_{-18}$ cm^{-3}, $\theta_j = 0.20^{+0.18}_{-0.16}$ rad and $\theta_{obs} = 0.12^{+0.21}_{-0.12}$ rad).

0.01 fits is minimal, and in the case of GRB 160509A, so is the difference between $\xi = 1$ and $\xi = 0.01$; thus, we cannot reliably distinguish between these scenarios. In the literature, it is commonly assumed that $\xi = 1$, and high values of η are obtained: for example, Lloyd-Ronning & Zhang (2004) find values as high as $\eta \sim 1$ depending on E_{iso}, and mostly $\eta \gtrsim 0.3$. Such a high efficiency is used as a criterion for successful models of prompt emission: e.g. the internal shock mechanism tends to result in $\eta \lesssim 0.1$ (Kumar & Zhang 2015, and references therein). Our results may indicate that, if very low values of ξ are more realistic (Warren et al. 2018), one should not dismiss models based on low efficiency.

5. CONCLUSIONS

We have presented our late-time optical, radio and X-ray observations of the afterglows of GRB 160625B and GRB 160509A. We have fitted broken power law functions to the data, combined with light curves from the literature, to constrain the jet break time and the post-jet-break decline, and used the numerical afterglow fitting software BOXFIT (van Eerten et al. 2012) to constrain the physical parameters and energetics of the two bursts. Our conclusions are as follows:

Regardless of the sharpness of the GRB 160625B jet break, we find that the effect of the jet edges becoming visible as the jet decelerates is alone insufficient to explain the post-jet-break light curves. A full lateral expansion break onto a t^{-p} decline is also inconsistent with the favored sharp break. The light curve behavior seems qualitatively consistent with the edge effect combined with only a fraction of the jet expanding at the speed of sound (van Eerten & MacFadyen 2012). It is also possible that an intrinsic scatter in the electron Lorentz factor distribution index p exists, the result of simplified synchrotron theory and closure relations that do not necessarily reflect the true complexity of the emission region (Gompertz et al. 2018). This scenario combined with lateral expansion is also consistent with our results. For GRB160509A we are unable to exclude any of the considered scenarios due to the scarcity of the available data.

Based on the best fits from BOXFIT, the geometry-corrected energy requirements of both GRBs are consistent with a magnetar spin-down energy source – albeit only in extreme cases when the 'participation fraction' (fraction of electrons accelerated into a non-thermal distribution) is fixed at $\xi = 0.1$ or $\xi = 0.01$, requiring energies of $\sim 3 \times 10^{52}$ or even $\sim 10^{53}$ erg. As simulations have shown these lower fractions to be more realistic (e.g. Warren et al. 2018), it seems that magnetar spin-down alone struggles to produce the required energies unless the nascent magnetar has extreme properties (Metzger et al. 2015).

However, neither BOXFIT nor analytical relations from standard jet theory (e.g. Rhoads 1999; Granot & Sari 2002) can provide a good fit to the radio data of either GRB, which are consistent with a single power law that requires the jet break to occur much later in radio than in the other bands. Both GRBs also show an almost flat radio SED at relatively late times (tens of days; see Laskar et al. 2016; Alexander et al. 2017). The higher frequencies do conform to expectations from the jet model, though. This might be the result of a multi-component jet, but that would require the wide component of the jet to dominate the light curve, and simultaneously suppressed flux from the narrow component. A similar behavior (a radio decline described by a single power law with $\alpha = -1.19 \pm 0.06$ until ~ 60 d) was recently reported for GRB 171010A by Bright et al. (2019). We explore this problem further in a companion paper (Kangas & Fruchter 2019), and find that these GRBs are not exceptional in this regard.

We thank the anonymous referee for comments that improved the paper. We also thank Hendrik van Eerten, Geoffrey Ryan, Alexander van der Horst, Paz Beniamini and Chryssa Kouveliotou for helpful discussions.

A.Co. acknowledges support from the National Science Foundation via CAREER award #1455090. A.dU.P. acknowledges support from a Ramon y Cajal fellowship (RyC-2012-09975), from the Spanish research project AYA2017-89384-P, and from the State Agency for Research of the Spanish MCIU through the "Center of Excellence Severo Ochoa" award for the Instituto de Astrofísica de Andalucía (SEV-2017-0709). A.P. wishes to acknowledge support by the European Research Council via the ERC consolidating grant #773062 (acronym O.M.J.). A.Cu. acknowledges the support of NASA MIRO grant NNX15AP95A.

Based on observations made with the NASA/ESA *Hubble Space Telescope* (programme GO 14353, PI Fruchter), obtained through the data archive at the Space Telescope Science Institute (STScI). STScI is operated by the Association of Universities for Research in Astronomy, Inc. under NASA contract NAS 5-26555. Support for this work was also provided by the National Aeronautics and Space Administration through Chandra Award Number 17500753, PI Fruchter, issued by the Chandra X-ray Center, which is operated by the Smithsonian Astrophysical Observatory for and on be-half of the National Aeronautics Space Administration under contract NAS8-03060.

This work made use of data supplied by the UK Swift Science Data Centre at the University of Leicester as well as observations made with the Gran Telescopio Canarias (GTC), installed in the Spanish Observatorio del Roque de los Muchachos of the Instituto de Astrofísica de Canarias, in the island of La Palma. Development of CIRCE was supported by the University of Florida and the National Science Foundation (grant AST-0352664), in collaboration with IUCAA.

The National Radio Astronomy Observatory is a facility of the National Science Foundation operated under cooperative agreement by Associated Universities, Inc.

Development of the boxfit code was supported in part by NASA through grant NNX10AF62G issued through the Astrophysics Theory Program and by the NSF through grant AST-1009863. Simulations for boxfit version 2 have been carried out in part on the computing facilities of the Computational Center for Particle and Astrophysics (C2PAP) of the research cooperation "Excellence Cluster Universe" in Garching, Germany.

Facilities: *HST*(WFC3), *Chandra*(ACIS-S), VLA, GTC(CIRCE)

Software: drizzlepac (Hack et al. 2013); pyraf (Science Software Branch at STScI 2012); iraf (Tody 1986); ciao (Fruscione et al. 2006); casa (McMullin et al. 2007); isis (Alard 2000; Alard & Lupton 1998); boxfit (van Eerten et al. 2012)

REFERENCES

Alard, C. 2000, A&AS, 144, 363, doi: 10.1051/aas:2000214

Alard, C., & Lupton, R. H. 1998, ApJ, 503, 325, doi: 10.1086/305984

Alexander, K. D., Laskar, T., Berger, E., et al. 2017, ApJ, 848, 69, doi: 10.3847/1538-4357/aa8a76

Amati, L., Frontera, F., Tavani, M., et al. 2002, A&A, 390, 81, doi: 10.1051/0004-6361:20020722

Bednarz, J., & Ostrowski, M. 1998, Physical Review Letters, 80, 3911, doi: 10.1103/PhysRevLett.80.3911

Bennett, C. L., Larson, D., Weiland, J. L., & Hinshaw, G. 2014, ApJ, 794, 135, doi: 10.1088/0004-637X/794/2/135

Berger, E., Kulkarni, S. R., Pooley, G., et al. 2003, Nature, 426, 154, doi: 10.1038/nature01998

Bright, J. S., Horesh, A., van der Horst, A. J., et al. 2019, MNRAS, 486, 2721, doi: 10.1093/mnras/stz1004

Bucciantini, N., Quataert, E., Arons, J., Metzger, B. D., & Thompson, T. A. 2008, MNRAS, 383, L25, doi: 10.1111/j.1745-3933.2007.00403.x

Bucciantini, N., Quataert, E., Metzger, B. D., et al. 2009, MNRAS, 396, 2038, doi: 10.1111/j.1365-2966.2009.14940.x

Cardelli, J. A., Clayton, G. C., & Mathis, J. S. 1989, ApJ, 345, 245, doi: 10.1086/167900

Cenko, S. B., Troja, E., & Tegler, S. 2016, GRB Coordinates Network, Circular Service, No. 19416, #1 (2016), 19416

Cenko, S. B., Frail, D. A., Harrison, F. A., et al. 2011, ApJ, 732, 29, doi: 10.1088/0004-637X/732/1/29

De Pasquale, M., Page, M. J., Kann, D. A., et al. 2016, MNRAS, 462, 1111, doi: 10.1093/mnras/stw1704

Dirirsa, F., Racusin, J., McEnery, J., & Desiante, R. 2016, GRB Coordinates Network, Circular Service, No. 19580, #1 (2016), 19580

Eikenberry, S. S., Charcos, M., Edwards, M. L., et al. 2018, Journal of Astronomical Instrumentation, 7, 1850002, doi: 10.1142/S2251171718500022

Evans, P. A., Beardmore, A. P., Page, K. L., et al. 2007, A&A, 469, 379, doi: 10.1051/0004-6361:20077530

—. 2009, MNRAS, 397, 1177, doi: 10.1111/j.1365-2966.2009.14913.x

Fraija, N., Veres, P., Zhang, B. B., et al. 2017, ApJ, 848, 15, doi: 10.3847/1538-4357/aa8a72

Frail, D. A., Waxman, E., & Kulkarni, S. R. 2000, The Astrophysical Journal, 537, 191, doi: 10.1086/309024

Fruchter, A. S., & Hook, R. N. 2002, PASP, 114, 144, doi: 10.1086/338393

Fruscione, A., McDowell, J. C., Allen, G. E., et al. 2006, in Proc. SPIE, Vol. 6270, Society of Photo-Optical Instrumentation Engineers (SPIE) Conference Series, 62701V

Gallant, Y. A., Achterberg, A., & Kirk, J. G. 1999, A&AS, 138, 549, doi: 10.1051/aas:1999503

Gompertz, B., & Fruchter, A. 2017, ApJ, 839, 49, doi: 10.3847/1538-4357/aa6629

Gompertz, B. P., Fruchter, A. S., & Pe'er, A. 2018, ArXiv e-prints. https://arxiv.org/abs/1802.07730

Granot, J., & Piran, T. 2012, MNRAS, 421, 570, doi: 10.1111/j.1365-2966.2011.20335.x

Granot, J., & Sari, R. 2002, ApJ, 568, 820, doi: 10.1086/338966

Grupe, D., Burrows, D. N., Wu, X.-F., et al. 2010, ApJ, 711, 1008, doi: 10.1088/0004-637X/711/2/1008

Güver, T., & Özel, F. 2009, MNRAS, 400, 2050, doi: 10.1111/j.1365-2966.2009.15598.x

Hack, W. J., Dencheva, N., & Fruchter, A. S. 2013, Astronomical Society of the Pacific Conference Series, Vol. 475, DrizzlePac: Managing Multi-component WCS Solutions for HST Data, ed. D. N. Friedel, 49

Hajela, A., Margutti, R., Alexander, K. D., et al. 2019, ApJL, 886, L17, doi: 10.3847/2041-8213/ab5226

Hancock, P. J., Gaensler, B. M., & Murphy, T. 2013, ApJ, 776, 106, doi: 10.1088/0004-637X/776/2/106

Hjorth, J., & Bloom, J. S. 2012, The Gamma-Ray Burst - Supernova Connection, ed. C. Kouveliotou, R. A. M. J. Wijers, & S. Woosley, 169–190

Iwamoto, K., Mazzali, P. A., Nomoto, K., et al. 1998, Nature, 395, 672, doi: 10.1038/27155

Kangas, T., & Fruchter, A. 2019, arXiv e-prints, arXiv:1911.01938. https://arxiv.org/abs/1911.01938

Kann, D. A., Klose, S., & Zeh, A. 2006, ApJ, 641, 993, doi: 10.1086/500652

Kirk, J. G., Guthmann, A. W., Gallant, Y. A., & Achterberg, A. 2000, ApJ, 542, 235, doi: 10.1086/309533

Krühler, T., Greiner, J., Schady, P., et al. 2011, A&A, 534, A108, doi: 10.1051/0004-6361/201117428

Kumar, P. 2000, ApJL, 538, L125, doi: 10.1086/312821

Kumar, P., & Zhang, B. 2015, PhR, 561, 1, doi: 10.1016/j.physrep.2014.09.008

Laskar, T., Alexander, K. D., Berger, E., et al. 2016, ApJ, 833, 88, doi: 10.3847/1538-4357/833/1/88

Liang, E.-W., Zhang, B.-B., & Zhang, B. 2007, ApJ, 670, 565, doi: 10.1086/521870

Lloyd-Ronning, N. M., Gompertz, B., Pe'er, A., Dainotti, M., & Fruchter, A. 2019, ApJ, 871, 118, doi: 10.3847/1538-4357/aaf6ac

Lloyd-Ronning, N. M., & Zhang, B. 2004, ApJ, 613, 477, doi: 10.1086/423026

Longo, F., Bissaldi, E., Bregeon, J., et al. 2016a, GRB Coordinates Network, Circular Service, No. 19403, #1 (2016), 19403

Longo, F., Bissaldi, E., Vianello, G., et al. 2016b, GRB Coordinates Network, Circular Service, No. 19413, #1 (2016), 19413

Lü, H.-J., & Zhang, B. 2014, ApJ, 785, 74, doi: 10.1088/0004-637X/785/1/74

Lü, H.-J., Lü, J., Zhong, S.-Q., et al. 2017, ApJ, 849, 71, doi: 10.3847/1538-4357/aa8f99

Lyutikov, M. 2012, MNRAS, 421, 522, doi: 10.1111/j.1365-2966.2011.20331.x

MacFadyen, A. I., & Woosley, S. E. 1999, ApJ, 524, 262, doi: 10.1086/307790

McMullin, J. P., Waters, B., Schiebel, D., Young, W., & Golap, K. 2007, in Astronomical Society of the Pacific Conference Series, Vol. 376, Astronomical Data Analysis Software and Systems XVI, ed. R. A. Shaw, F. Hill, & D. J. Bell, 127

Melandri, A., D'Avanzo, P., D'Elia, V., et al. 2016, GRB Coordinates Network, Circular Service, No. 19585, #1 (2016), 19585

Mészáros, P., & Rees, M. J. 1999, MNRAS, 306, L39, doi: 10.1046/j.1365-8711.1999.02800.x

Metzger, B. D., Margalit, B., Kasen, D., & Quataert, E. 2015, MNRAS, 454, 3311, doi: 10.1093/mnras/stv2224

Nakar, E., Ando, S., & Sari, R. 2009, The Astrophysical Journal, 703, 675, doi: 10.1088/0004-637X/703/1/675

Oke, J. B., & Gunn, J. E. 1983, ApJ, 266, 713, doi: 10.1086/160817

Paczynski, B. 1986, ApJL, 308, L43, doi: 10.1086/184740

Paczynski, B., & Rhoads, J. E. 1993, ApJL, 418, L5, doi: 10.1086/187102

Panaitescu, A., & Mészáros, P. 1999, ApJ, 526, 707, doi: 10.1086/308005

Pei, Y. C. 1992, ApJ, 395, 130, doi: 10.1086/171637

Peng, F., Königl, A., & Granot, J. 2005, ApJ, 626, 966, doi: 10.1086/430045

Piran, T. 2004, Reviews of Modern Physics, 76, 1143, doi: 10.1103/RevModPhys.76.1143

Racusin, J. L., Liang, E. W., Burrows, D. N., et al. 2009, ApJ, 698, 43, doi: 10.1088/0004-637X/698/1/43

Rhoads, J. E. 1999, ApJ, 525, 737, doi: 10.1086/307907

Roberts, O. J., Fitzpatrick, G., & Veres, P. 2016, GRB Coordinates Network, 19411, 1

Ryan, G., van Eerten, H., MacFadyen, A., & Zhang, B.-B. 2015, ApJ, 799, 3, doi: 10.1088/0004-637X/799/1/3

Sari, R., Piran, T., & Halpern, J. P. 1999, ApJL, 519, L17, doi: 10.1086/312109

Sari, R., Piran, T., & Narayan, R. 1998, ApJL, 497, L17, doi: 10.1086/311269

Schady, P., Dwelly, T., Page, M. J., et al. 2012, A&A, 537, A15, doi: 10.1051/0004-6361/201117414

Schlafly, E. F., & Finkbeiner, D. P. 2011, ApJ, 737, 103, doi: 10.1088/0004-637X/737/2/103

Science Software Branch at STScI. 2012, PyRAF: Python alternative for IRAF. http://ascl.net/1207.011

Sironi, L., & Spitkovsky, A. 2011, ApJ, 726, 75, doi: 10.1088/0004-637X/726/2/75

Sironi, L., Spitkovsky, A., & Arons, J. 2013, ApJ, 771, 54, doi: 10.1088/0004-637X/771/1/54

Skrutskie, M. F., Cutri, R. M., Stiening, R., et al. 2006, AJ, 131, 1163, doi: 10.1086/498708

Strausbaugh, R., Butler, N., Lee, W. H., Troja, E., & Watson, A. M. 2018, ArXiv e-prints. https://arxiv.org/abs/1810.08852

Svinkin, D., Golenetskii, S., Aptekar, R., et al. 2016, GRB Coordinates Network, Circular Service, No. 19604, #1 (2016), 19604

Tanvir, N. R., Levan, A. J., Cenko, S. B., et al. 2016, GRB Coordinates Network, Circular Service, No. 19419, #1 (2016), 19419

Tody, D. 1986, Society of Photo-Optical Instrumentation Engineers (SPIE) Conference Series, Vol. 627, The IRAF Data Reduction and Analysis System, ed. D. L. Crawford, 733

Troja, E., Lipunov, V. M., Mundell, C. G., et al. 2017, Nature, 547, 425, doi: 10.1038/nature23289

van der Horst, A. J. 2007, PhD thesis, University of Amsterdam

van der Horst, A. J., Kamble, A., Resmi, L., et al. 2008, Astronomy and Astrophysics, 480, 35, doi: 10.1051/0004-6361:20078051

van Eerten, H., van der Horst, A., & MacFadyen, A. 2012, ApJ, 749, 44, doi: 10.1088/0004-637X/749/1/44

van Eerten, H. J., & MacFadyen, A. I. 2012, ApJ, 751, 155, doi: 10.1088/0004-637X/751/2/155

Wang, Y.-Z., Wang, H., Zhang, S., et al. 2017, ApJ, 836, 81, doi: 10.3847/1538-4357/aa56c6

Warren, D. C., Barkov, M. V., Ito, H., Nagataki, S., & Laskar, T. 2018, MNRAS, 480, 4060, doi: 10.1093/mnras/sty2138

Willingale, R., Starling, R. L. C., Beardmore, A. P., Tanvir, N. R., & O'Brien, P. T. 2013, MNRAS, 431, 394, doi: 10.1093/mnras/stt175

Woosley, S. E. 1993, ApJ, 405, 273, doi: 10.1086/172359

Woosley, S. E., & Bloom, J. S. 2006, ARA&A, 44, 507, doi: 10.1146/annurev.astro.43.072103.150558

Xu, D., Malesani, D., Fynbo, J. P. U., et al. 2016, GRB Coordinates Network, Circular Service, No. 19600, #1 (2016), 19600

Zhang, B., Fan, Y. Z., Dyks, J., et al. 2006, ApJ, 642, 354, doi: 10.1086/500723

Zhang, B.-B., Zhang, B., Castro-Tirado, A. J., et al. 2018, Nature Astronomy, 2, 69, doi: 10.1038/s41550-017-0309-8

Zhang, W., & MacFadyen, A. I. 2006, ApJS, 164, 255, doi: 10.1086/500792